Journal of Oceanology and Limnology
Vol. 36 No. 2, P. 216-229, 2018
https://doi.org/10.1007/s00343-018-6302-y

A numerical study of the South China Sea Warm Current during winter monsoon relaxation*

ZHANG Cong (张丛)[1, 2], DING Yang (丁扬)[2, **], BAO Xianwen (鲍献文)[1, 2], BI Congcong (毕聪聪)[1, 2], LI Ruixiang (李锐祥)[3], ZHANG Cunjie (张存杰)[1, 2], SHEN Biao (沈飙)[2], WAN Kai (万凯)[4]

[1] *College of Oceanic and Atmospheric Sciences, Ocean University of China, Qingdao 266100, China*

[2] *Key Laboratory of Physical Oceanography, Ministry of Education, Ocean University of China, Qingdao 266100, China*

[3] *South China Sea Marine Survey and Technology Center, State Ocean Administration, Guangzhou 510310, China*

[4] *Beihai Offshore Engineering Survey Institute, State Oceanic Administration, Qingdao 266061, China*

Received Nov. 17, 2016; accepted in principle Jan. 4, 2017; accepted for publication Feb. 27, 2017

Abstract Using a Finite-Volume Community Ocean Model, we investigated the dynamic mechanism of the South China Sea Warm Current (SCSWC) in the northern South China Sea (NSCS) during winter monsoon relaxation. The model reproduces the mean surface circulation of the NSCS during winter, while model-simulated subtidal currents generally capture its current pattern. The model shows that the current over the continental shelf is generally southwestward, under a strong winter monsoon condition, but a northeastward counter-wind current usually develops between 50- and 100-m isobaths, when the monsoon relaxes. Model experiments, focusing on the wind relaxation process, show that sea level is elevated in the northwestern South China Sea (SCS), related to the persistent northeasterly monsoon. Following wind relaxation, a high sea level band builds up along the mid-shelf, and a northeastward current develops, having an obvious vertical barotropic structure. Momentum balance analysis indicates that an along-shelf pressure gradient provides the initial driving force for the SCSWC during the first few days following wind relaxation. The SCSWC subsequently reaches a steady quasi-geostrophic balance in the cross-shelf direction, mainly linked to sea level adjustment over the shelf. Lagrangian particle tracking experiments show that both the southwestward coastal current and slope current contribute to the northeastward movement of the SCSWC during winter monsoon relaxation.

Keyword: northern South China Sea; South China Sea Warm Current; monsoon relaxation; numerical model; pressure gradient; barotropic structure

1 INTRODUCTION

The South China Sea (SCS) is semi-enclosed; it is the largest marginal Sea in the western Pacific Ocean. The northern South China Sea (NSCS) features a broad shallow continental shelf, with a width of 200–300 km and narrow steep slope, where bathymetry deepens rapidly from 300 to 3 000 m (Fig.1). Driven by the East Asian monsoon wind, the upper ocean circulation in the SCS has a dramatic seasonal variability (Wyrtki, 1961). During winter, the currents over the NSCS continental shelf generally flow southwestward, when the northeasterly monsoon is prevailing. However, in-situ observations indicate that a northeastward current, flowing against the wind often exists over the shelf break (Guan, 1978, 1985; Guo et al., 1985; Fang and Zhao, 1988; Zhong, 1990). This winter counter-wind current was first described by Guan and Chen (1964) in the NSCS, and was named the South China Sea Warm Current (SCSWC) because of its higher temperature compared with surrounding waters. A detailed review of the characteristics and dynamic mechanisms of the SCSWC is given by Guan and Fang (2006).

* Supported by the National Natural Science Foundation of China (Nos. 41606005, 41430963), the National Science Foundation for Post-Doctoral Scientists of China (No. 2015M582133), and the Fundamental Research Funds for the Central Universities (No. 201713023)
** Corresponding author: dingyangpol@ouc.edu.cn

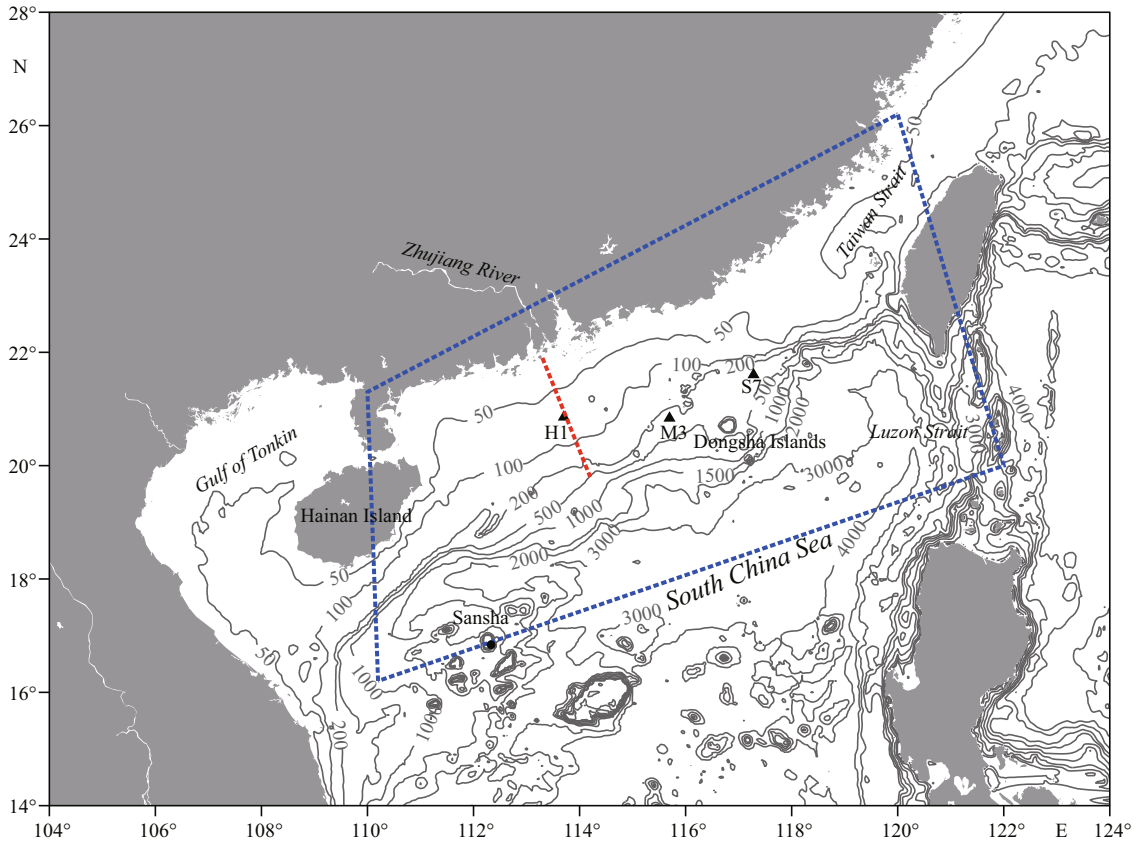

Fig.1 Map of the northern South China Sea

Contours indicate isobaths in meters. The red dashed line denotes a transect, west of the Zhujiang River estuary. The blue dashed box denotes the region used for numerical experiments on the effects of different wind forcing patterns. M3, H1 and S7 give the locations of the moored acoustic Doppler current profilers that provided data used in this study.

Based on limited observations and numerical models, two primary mechanisms for the generation of the SCSWC were proposed. Many oceanographers attributed the occasional winter monsoon relaxation to be the trigger mechanism for the SCSWC. Chao et al. (1995) demonstrated that water piles up in the southwest region of the SCS under the strong northeasterly wind condition prevailing during winter. When the winter monsoon weakens, a northeastward current develops along the northwestern continental shelf, driven by a sea level gradient between southwestern and northeastern regions of the SCS. Yang (2006) analyzed moored acoustic Doppler current profiler (ADCP) data, showing that the SCSWC was not persistent, existing only during relaxation of the winter monsoon. Chiang et al. (2008) also suggested that the occasional winter monsoon relaxation was the dominant mechanism, and that the Kuroshio intrusion had only a minor contribution to the SCSWC. They argued that the elevated sea level in the Gulf of Tonkin, induced by the northeasterly monsoon, was the ultimate driving force for the SCSWC during monsoon relaxation. The Kuroshio intrusion is also considered a cause of the SCSWC. Numerical experiments were performed to show that the Kuroshio intrusion through the Luzon Strait and the South China Sea Branch of Kuroshio (SCSBK) were necessary conditions for the formation of the SCSWC (Wang and Fang, 2001; Wang et al., 2001). Hsueh and Zhong (2004) suggested that the along-shelf break pressure distribution induced by the collision of the Kuroshio intrusion with the continental slope provided the driving force for the northeastward SCSWC. Xue et al. (2004) also suggested that the intruded Kuroshio water induced an upwelling over the upper slope, creating barotropic and baroclinic pressure gradients that support the northeastward SCSWC.

There are also other opinions on the formation mechanism of the SCSWC. Yang et al. (2008) investigated the relationship between the SCSWC and the Taiwan Strait Current, using a one-layer barotropic ocean circulation model. They showed that neither the wind stress forcing nor the Kuroshio intrusion was main forcing mechanism of the SCSWC. Instead, they considered it a source- and

sink-driven flow. Wang et al. (2010) suggested that the onshore-veered slope current, related to the joint effects of baroclinicity and relief (JEBAR), provided the major mass source for the SCSWC. Furthermore, Wang et al. (2011) suggested that the SCSWC was driven by Ekman pumping in the west, while the Kuroshio intrusion played a more crucial role in the east.

Long-term observations in the NSCS over winter have failed to capture the continuous SCSWC over the continental shelf (Yang, 2006; He et al., 2012; Xiong, 2013; Li et al., 2014). Such observations lead to various research questions: Is the SCSWC a permanent winter feature or does it only exist during winter monsoon relaxation? What are the main dynamic factors contributing to the SCSWC, and how do they relate to the winter monsoon? To our knowledge, these questions still need to be addressed.

In this paper, we attempt to investigate the dynamic mechanisms behind the SCSWC during winter monsoon relaxation. Our manuscript is organized, as follows. In Section 2, we briefly describe the observations and model used in this study. Section 3 presents results of our modeling, as model-data comparisons. A numerical experiment and an analysis of the momentum budget were also carried out. These analyses help us define the characteristics and formation mechanisms of the SCSWC during the winter monsoon relaxation. We also discuss the mass source of the SCSWC in this section, based on Lagrangian particle tracking experiments. Section 4 contains our conclusions.

2 DATA AND MODELING APPROACH

Our investigations of the SCSWC are based directly on long-term moored ADCP data. The data obtained mainly from one moored ADCP (M3) over the winter months was used for analysis and model validation in this study. M3 was deployed on the mid-shelf, having a water depth of around 280 m (Fig.1). Detailed information on M3 is given in Table 1 of Li et al. (2014).

The wind stress obtained from Ocean General Circulation Model for the Earth Simulator (OFES) has a time interval of three days and a spatial resolution of 0.5°×0.5°; while wind speed from the Cross-Calibrated Multi-Platform (CCMP) has a time interval of 6 hours and a spatial resolution of 0.25°×0.25°. Both were used to analyze the characteristics of the SCSWC during monsoon relaxation and to force the model.

Daily high-resolution sea surface temperature (SST) derived from AVHRR Pathfinder V5.2 (obtained from the US National Oceanographic Data Center; http://pathfinder.nodc.noaa.gov), and the NOAA OI SST V2 High Resolution Dataset (obtained from the US national Oceanic and Atmospheric Administration; https://www.esrl.noaa.gov/psd/) were used for model assimilation.

The surface current data derived from Argo (Xie and Zhu, 2008, 2009) were used to analyze the winter circulation patterns of the NSCS and to validate the surface current structure of the model. These data, averaged from 1999 to 2010, were obtained from the China Argo Real-time Data Center.

Given the lack of long-term and large-scale direct current measurements in the NSCS, it is difficult to understand the characteristics and mechanisms of the SCSWC from field data. This prompted us to develop a numerical model to explore various mechanisms in this study; this model is built under the platform of the unstructured-grid Finite-Volume Community Ocean Model. The model domain covers the entire Pacific and part of the Indian Ocean, within the longitudinal range of 87°E–60°W and latitudinal range of 80°S–65°N. Open boundaries were set far away from the SCS. The large computational area reduces the effects induced by the uncertainty of these open boundaries and helps resolve interaction between the Pacific circulation system and SCS circulation system.

The model features a horizontal resolution of around 0.06–0.2° over the SCS. Our vertical grid is constructed using a 30-layer σ coordinate. The water depth of the open ocean in the model is based on topographic data from the Digital Bathymetric Data Base 5-minute (DBDB5; U.S. Naval Oceanographic Office, 1983); while the minimum and maximum depths in the model are set to be 7 and 5 500 m, respectively. The model is initialized using winter temperature and salinity data from OFES. The vertical and horizontal mixing processes are resolved using Mellor and Yamada level 2.5 (MY-2.5; Mellor and Yamada, 1982) and the Smagorinsky turbulence closure schemes (Smagorinsky, 1963), respectively. The model was spun up for ten years, before being run under realistic forcing conditions from 1999 to 2011.

The circulation in the SCS is influenced by many factors, including seasonal monsoon, topography, the Kuroshio intrusion, and heat budget. Both surface heat and freshwater flux have a significant influence

on the temperature and salinity distribution of the SCS. To better resolve the thermal dynamics of the SCS circulation, the surface forcing used to drive the model includes sea surface wind, surface heat, and freshwater flux. The surface wind field employed is a 6-hourly wind forcing, with a horizontal resolution of 0.25°×0.25° obtained from the CCMP. The heat and freshwater fluxes used have a daily interval, with a horizontal resolution of 1.875°×1.875° from National Centers of Environmental Prediction reanalysis. Daily subtidal elevation, temperature, and salinity from the Hybrid Coordinate Ocean Model (HYCOM) reanalysis data are applied as conditions on all open boundaries. Any discrepancy between model-simulated temperatures and observations occurring during the model run, as well as biases in surface temperature fields, will lead to errors in the model density (Chen and He, 2015). Therefore, the satellite-derived SST data are also assimilated into the model to correct for such biases and to better resolve the upper layer circulation. We believe that our model results are greatly improved by assimilating these data into our model (Zeng et al., 2014).

3 RESULT AND DISCUSSION

3.1 Model-data comparison of current behavior during winter

The current field at 10 m depth can be used to represent the upper circulation over the NSCS continental shelf in winter (Guan, 1986; Guan and Fang, 2006). Therefore, monthly mean surface current vectors estimated from Argo drifters (Xie and Zhu, 2008, 2009) were compared with the model-computed current vectors at 10 m depth during winter (Fig.2). In addition, the model-simulated currents were compared with HYCOM reanalysis data (Fig.2a, b, c). Generally, the model-simulated current data in the NSCS were similar to HYCOM reanalysis data. However, there were differences between current vectors estimated from Argo drifters and both our model and HYCOM reanalysis data, especially in shallow water areas, where Argos data may not be very accurate. Despite this, the monthly mean surface current pattern for the winter season from our model was consistent with the pattern calculated by Centurioni et al. (2009) using Argos data. It can be seen that on a monthly time scale, surface currents over the NSCS continental shelf are generally southwestward, and no steady northeastward current exists during winter.

Comparisons of the observed and model-computed subtidal currents at M3 are shown in Fig.3. The northeasterly wind at M3 was persistently strong and stable over this period, while the currents at 53 m depth were markedly affected by wind, and were southwestward; this was most obvious during January 2007. Currents were relatively weak at depths of 197 and 269 m. The model-simulated subtidal currents generally flowed southwestward, consistent with observations. Interestingly, the persistent northeastward SCSWC was not observed during this period. Mismatch between observations and model data reflect that model output data gives a daily mean, while observations are low-pass filtered data having a time interval of 6 hours. In addition, the model was run without tidal forcing. Finally, both inaccurate surface forcing and topography all contribute to a bias between model results and observations. In this paper, we focus our study on the northeastward current adjustment during winter monsoon relaxation. In this case, magnitude differences between our model data and observations do not affect our exploration of the dynamic mechanisms of the SCSWC or our conclusions.

3.2 Characteristics of the current during the northeasterly monsoon and its relaxation periods

The northeasterly winter monsoon over the SCS periodically weakens during the winter season. According to the observed low-pass filtered wind and current data at sites H1 and S7 during the winters of 2001–2002 and 2005–2006, respectively, the northeastward SCSWC was observed intermittently over the shelf or slope, corresponding to periods when the northeasterly monsoon weakened, such as in January 2002 and November 2005 (Yang, 2006). Previous studies (Guo et al., 1985; Guan, 1985, 1986; Wang et al., 2010) proposed that these periods correspond to a relatively weak northeasterly monsoon. These observations suggest that the northeastward SCSWC may respond to the relaxation of the northeasterly monsoon.

The satellite-derived surface-wind stress fields and the model-computed surface current fields at 10 m depth from 1 to 16 January 2002, having a time interval of 3 days are shown in Fig.4. The sea-surface elevation fields are superimposed on this figure. On 1 January, weak northeastward flow only occurred in the Taiwan Strait, while currents over the NSCS continental shelf were weak, except for a southwestward coastal current moving west of the Zhujiang (Pearl) River estuary. The current vectors

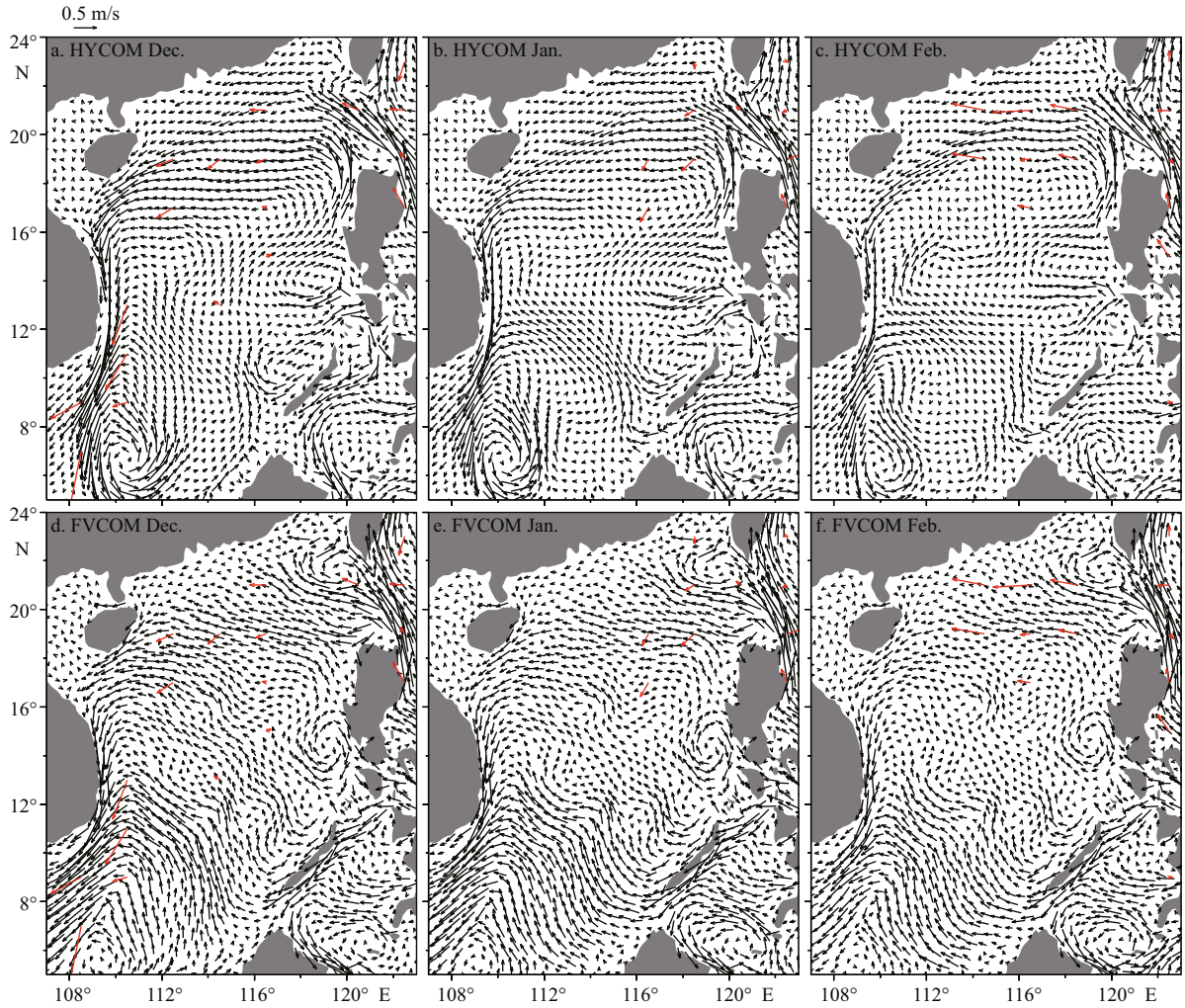

Fig.2 Maps of Hybrid Coordinate Ocean Model (HYCOM) reanalysis data (a, b, c) and our Finite-Volume Community Ocean Model (FVCOM) model-computed (d, e, f) monthly mean current vectors at 10 m depth in the South China Sea during winter

Red vectors denote observed monthly averaged current vectors at 10 m depth derived from Argos data.

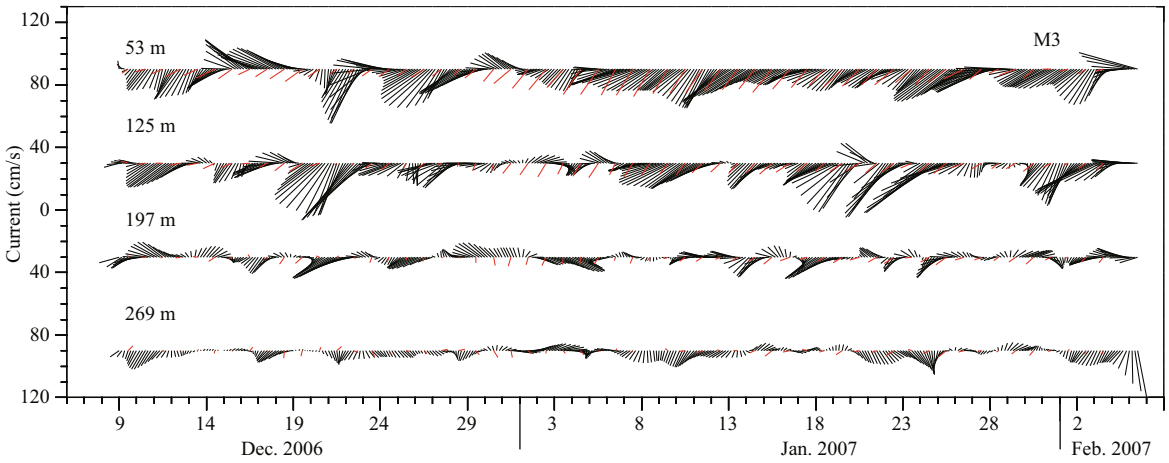

Fig.3 Time series of 33 h low-pass filtered observed (black) and model-computed daily (red) current vectors at profiler site M3 at depths of 53, 125, 197, and 269 m for the period from December 2006 to February 2007

The observational data are from Li et al. (2014).

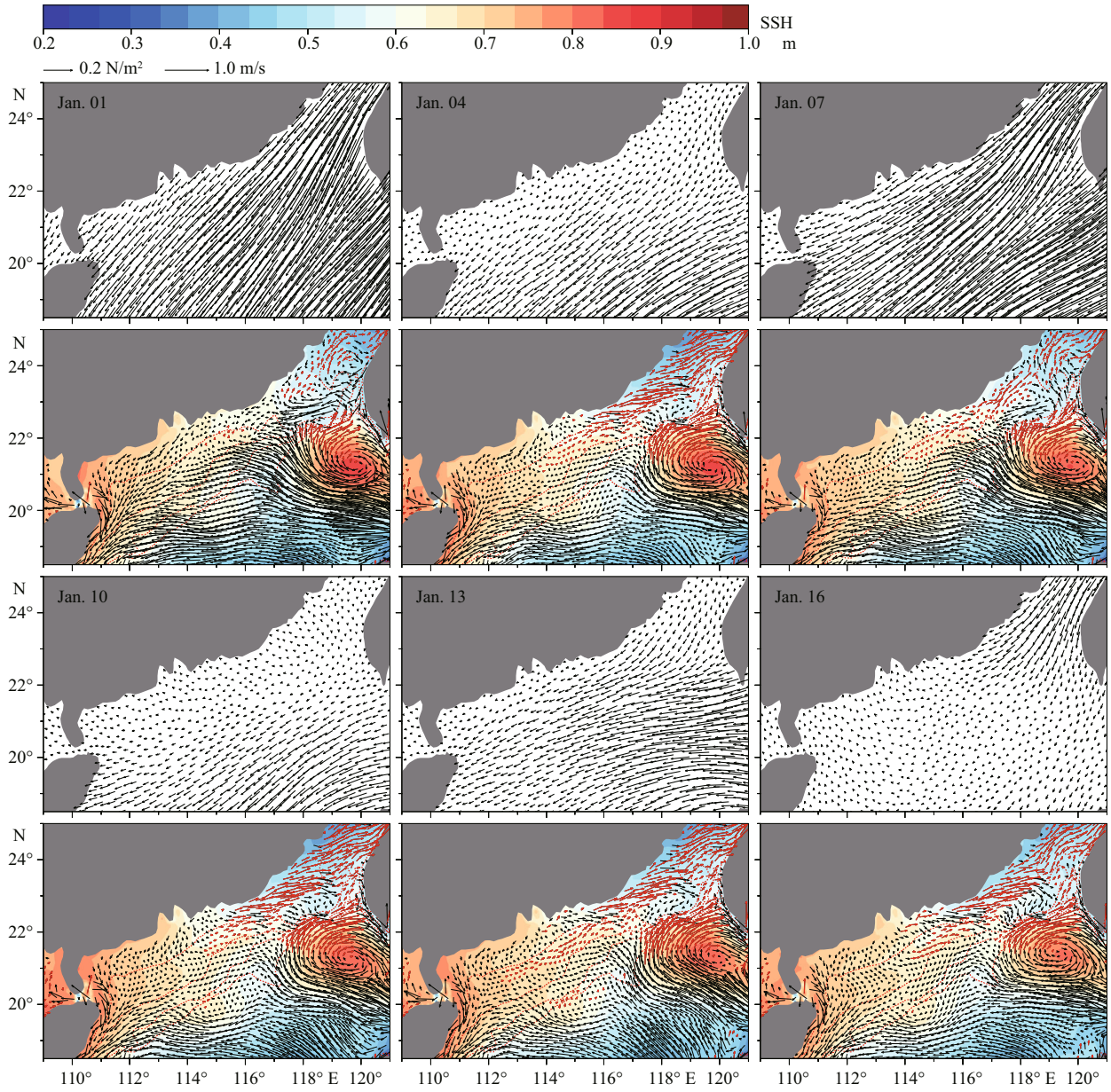

Fig.4 Maps of satellite-derived 10 m wind stress vectors and model-computed current vectors at 10 m depth superimposed on the sea surface elevation fields of the northern South China Sea for the period from 1 to 16 January 2002

Red arrows denote northeastward current vectors. Contours indicate isobaths of 50, 100, 200, and 400 m.

over the narrow shelf break at a depth range of 200–400 m were generally westward. On 4 January, the northeastward flow in the Taiwan Strait intensified, as the northeasterly wind weakened, and a northeastward flow occurred over the shelf east of 114°E. The intensity of the current in the southwest part of the Taiwan Strait was stronger than east of the Zhujiang River estuary. This is consistent with observations from a previous study (Guan, 2002). The northeastward current weakened as wind intensified on 7 January. From 10 to 16 January, because of persistent relaxation of the northeasterly wind, the northeastward SCSWC existed throughout this period, extending as far west as 112°E. High sea level occurred within the mid-shelf region between the 50- and 100-m isobaths, coincident with the northeastward SCSWC.

3.3 Numerical experiment results

To investigate the responses of the current over the NSCS continental shelf to the prevailing versus intermittent relaxation processes of the northeasterly monsoon, a numerical experiment was carried out. This involved rerunning the model for January 2002, while changing the local wind forcing fields over the

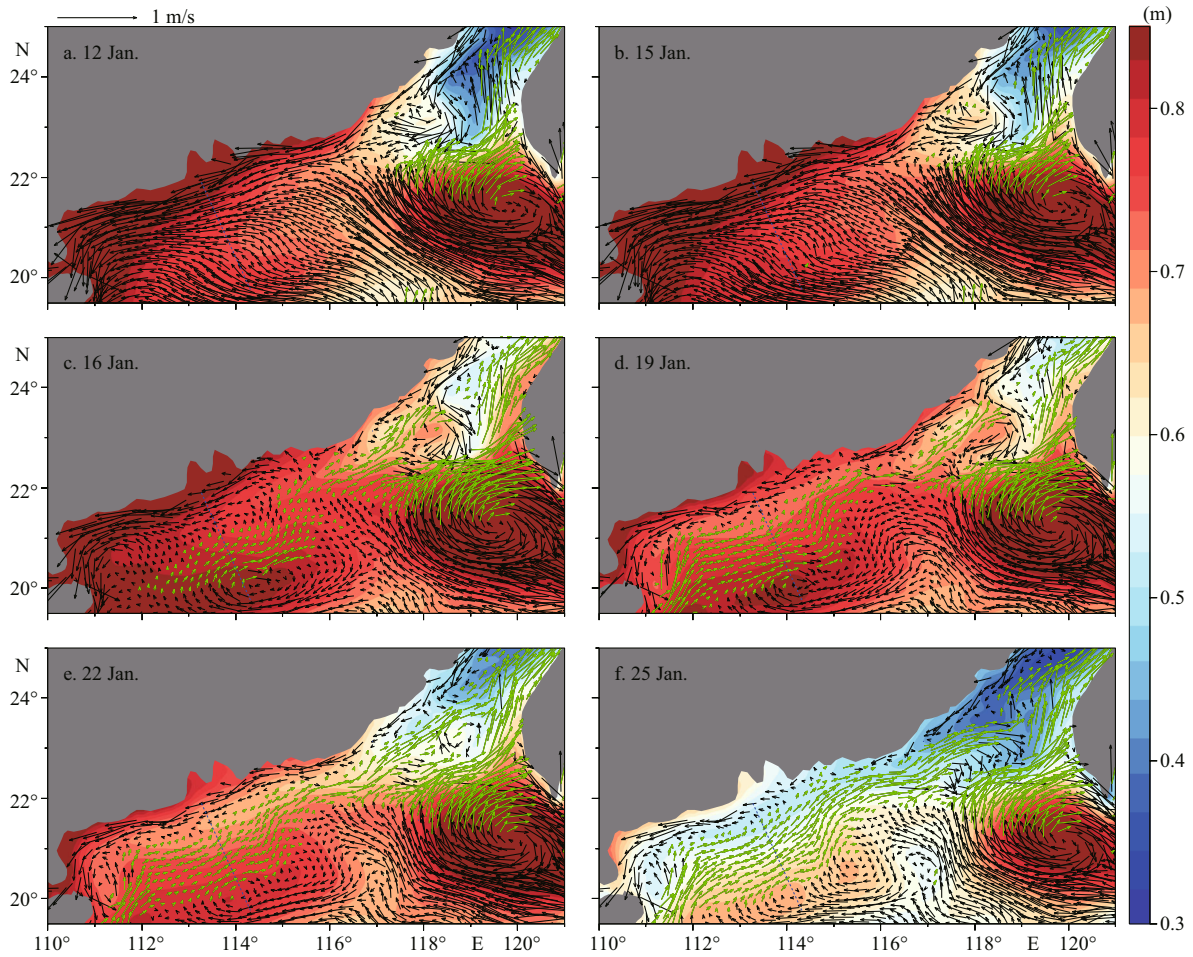

Fig.5 Maps of model-computed current vectors at 10 m depth superimposed on the corresponding sea surface height fields in the northern South China Sea before (12 and 15 January 2002) and after (16, 19, 22, and 25 January 2002) wind relaxation

Green arrows denote northeastward current vectors. The blue dashed line gives the location of the transect, west of the Zhujiang River estuary.

NSCS. We selected this month because we found that the northeasterly wind during January 2002 was typical of the winter monsoon relaxation pattern. The probability of northeasterly monsoon conditions, with a mean velocity of around 8–12 m/s, reaches more than 90% in the NSCS from October to February (Guan, 2002). Therefore, the wind speed within the blue box shown in Fig.1 was set to be uniform in space and time, with a speed of 10 m/s both in zonal and meridional directions from 1 to 15 January. It gradually attenuated from 16 January, maintaining a speed of 5 m/s from 17 to 31 January. All other external forcing was kept the same as the climatological simulation.

Figure 5 presents the simulated sea surface height (SSH) distributions and current fields at 10 m depth before (12 and 15 January) and after (16, 19, 22, and 25 January) wind relaxation. Before wind relaxation, the circulation pattern over the NSCS continental shelf was dominated by the winter monsoon and the Kuroshio intrusion. Currents generally flowed southwestward and northwestward, with no steady northeastward flow over the shelf. Because of persistent northeasterly forcing by the wind, water piled up in the northwestern area of the SCS, generating a steady SSH gradient towards the northeast (Fig.5a, b). There was a permanent northeastward current in the eastern part of the Taiwan Strait. On 16 January, when the northeasterly wind weakened, the current between the 50- and 100-m isobaths gradually rotated clockwise to flow northeastward against the wind. This northeastward current originated from 112°E, extending south of the Taiwan Strait, along isobaths. It gradually intensified from west to the east, with a velocity range of 10–30 cm/s (Fig.5c). Once the northeasterly wind attenuated to 5 m/s from 19 to 25 January, the SSH over the shelf began to decrease, although the

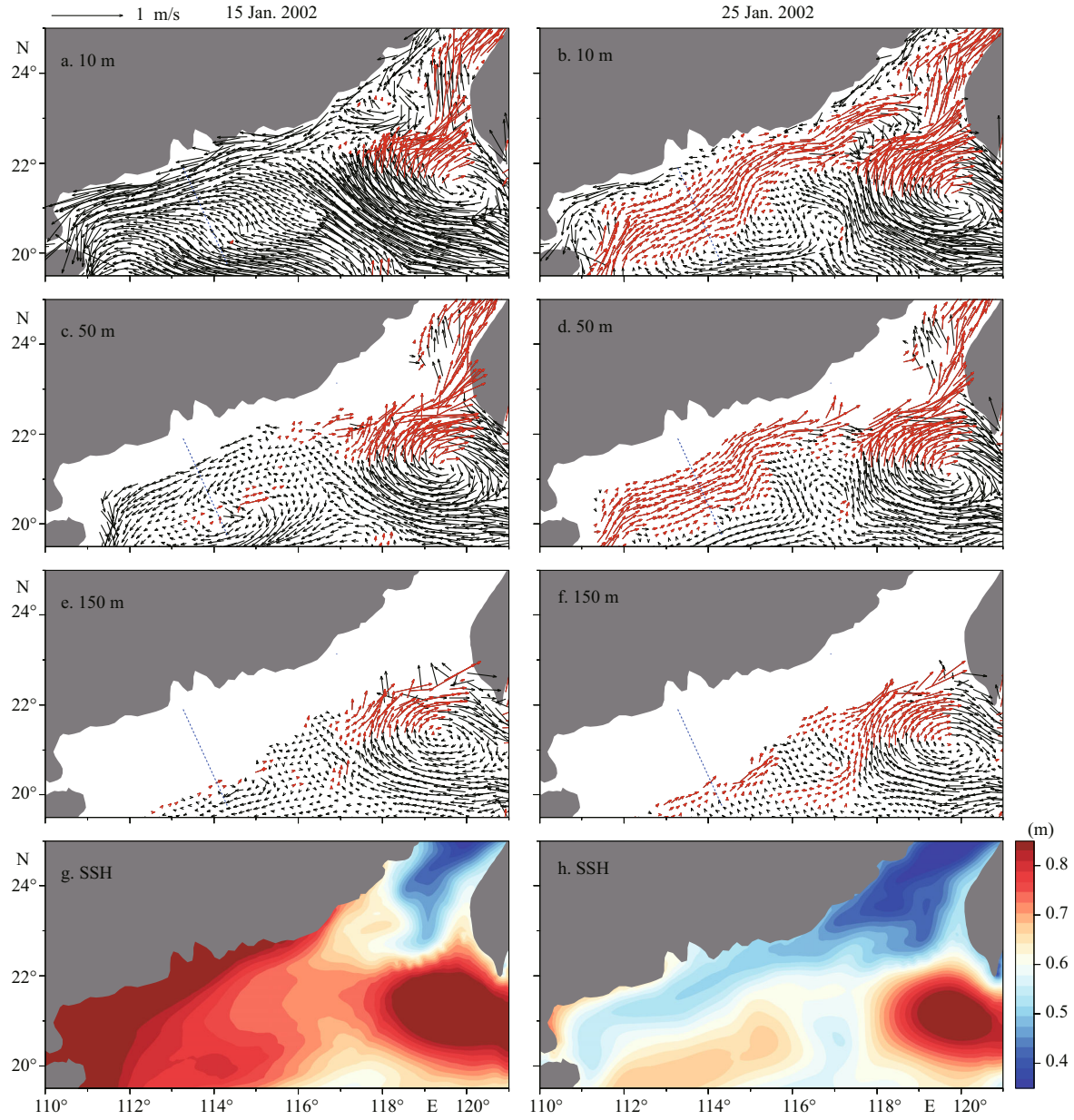

Fig.6 Maps of model-computed current vectors at depths of 10, 50, and 150 m and distributions of SSH in the northern South China Sea before (15 January 2002) and after (25 January 2002) wind relaxation

Red arrows denote northeastward current vectors. The blue dashed line shows the location of the transect, west of the Zhujiang River estuary.

northeastward current was still stable, extending from southeast of the Hainan Island to south of the Taiwan Strait (Fig.5d, e, f). Following wind relaxation, a high sea level developed along isobaths, and a strong cross-shelf SSH gradient occurred. As the wind condition continued to relax, the northeastward current intensified, connecting with the Taiwan Strait Current to form the winter counter-wind current system off the southeastern coast of China (Guan, 2002; Guan and Fang, 2006).

Two representative snapshots were selected to illustrate responses of the SSH and currents over the NSCS continental shelf before and after relaxation of the northeasterly monsoon and the vertical structure of the northeastward SCSWC. The northeasterly wind was strong and stable (10 m/s) on 15 January, but was weak (5 m/s) on 25 January. Figure 6 shows the simulated SSH distributions and current fields at depths of 10, 50, and 150 m in the NSCS for these two snapshots. A high SSH built up in the northwestern SCS and decreased seaward, as the northeasterly monsoon became persistently stronger (Fig.6g). On 15 January, the currents over the NSCS continental shelf were generally westward, and the velocities

decreased with depth (Fig.6a, c, e). There is no steady northeastward current at any layer of the model. Once the northeasterly wind relaxed, as is the case on 25 January, the shelf between the 50- and 150-m isobaths was dominated by the northeastward SCSWC, having an obvious barotropic vertical feature (Fig.6b, d, f). Furthermore, it can be seen in Fig.6h that SSH gradients existed in both along- and cross-shelf directions. The gradient in the cross-shelf direction was stronger than along the shelf, especially west of the Zhujiang River estuary, once the SCSWC reached a steady state.

Li et al. (2014) analyzed SSH data and current data from a mooring station in this region and found that an anti-cyclonic eddy was observed to move southwestward at a relatively constant speed, related to the westward propagation speed of Rossby waves. The current observations showed that this anticyclonic eddy affected local currents for more than a week, and induced a counter-wind northeastward current. In addition to the winter monsoon, it is possible that mesoscale eddies propagating westwards in the NSCS also affect the SCSWC. Further observations and high-resolution eddy-resolving models are required to investigate the effects of such eddies on the SCSWC.

3.4 Momentum balance analysis

Both observations and model experiments show that relaxation of the northeasterly monsoon plays an important role in generating the SCSWC. A momentum balance analysis was carried out to determine the dynamic mechanisms of the SCSWC during winter wind relaxation. A transect west of the Zhujiang River estuary (Fig.1) was selected for analysis. Each term of the two momentum equations was examined during the monsoon relaxation process along this transect.

The along-shelf (x) and cross-shelf (y) momentum equations can be represented by:

$$-fv+\mathrm{g}\frac{\partial\zeta}{\partial x}+\frac{1}{\rho}\frac{\partial p}{\partial x}+\vec{V}\cdot\nabla u+ w\frac{\partial u}{\partial z}-\frac{\partial}{\partial z}\left(K_m\frac{\partial u}{\partial z}\right)-F_u+\frac{\partial u}{\partial t}=0, \quad (1)$$

$$fu+\mathrm{g}\frac{\partial\zeta}{\partial y}+\frac{1}{\rho}\frac{\partial p}{\partial y}+\vec{V}\cdot\nabla v+ w\frac{\partial v}{\partial z}-\frac{\partial}{\partial z}\left(K_m\frac{\partial v}{\partial z}\right)-F_v+\frac{\partial v}{\partial t}=0, \quad (2)$$

where $\vec{V}$ is the velocity vector with components (u, v); f is the Coriolis parameter; ζ is the sea level fluctuation; g is gravitational acceleration; ρ is seawater density; p is the pressure induced by the density gradient; K_m is the vertical viscosity coefficient; and F_u and F_v represent the horizontal diffusion terms along- and cross-shelf, respectively. The terms in the momentum equations from left to right are: (a) the Coriolis term, (b) the barotropic pressure gradient term, (c) the baroclinic pressure gradient term, (d) the horizontal advection term, (e) the vertical advection term, (f) the vertical diffusion term, (g) the horizontal diffusion term, and (h) the time variation term.

Figure 7 shows the time series of the daily wind stress, current vectors, and momentum balance terms in the along- and cross-shelf directions for January 2002. During the first 14 days of January, the northeasterly wind was homogenous, while depth-integrated currents along the transect were generally southwestward. The barotropic pressure gradient term, together with the Coriolis term, vertical diffusion term, and time variation term were the dominant terms in the along-shelf direction. The contribution of the baroclinic pressure gradient term was small. In the cross-shelf direction, the dominant terms were the Coriolis term, time variation term, and barotropic pressure gradient term. When the northeasterly wind began to weaken on 15 January, the southwestward currents over the shelf began to turn northeastward against the wind. The along-shelf barotropic pressure gradient term was always positive (pointing to the northeast) after 15 January. Therefore, it could be the main driving force for the northeastward SCSWC, as the flow was generally ageostrophic along the shelf. In the cross-shelf direction, the current had a clearly quasi-geostrophic feature, with a balance between the Coriolis term and barotropic pressure gradient term. Thus, the baroclinic pressure gradient term, vertical diffusion term, and time variation term are still marked and cannot be ignored, once the wind weakens.

The variation in momentum terms during the wind relaxation process suggests that the barotropic pressure gradients in both along and cross-shelf directions play an important role in generating the northeastward SCSWC. Furthermore, collective wisdom from previous studies identifies these two terms as being important to generation scenarios during winter monsoon relaxation: 1) the cross-shelf pressure gradient (Su and Wang, 1987; Su and Liu, 1992; Xue et al., 2004; Hong and Wang, 2006) and 2) the along-shelf pressure gradient (Chao et al., 1995; Yang, 2006; Chiang et al., 2008). Figure 8 shows the

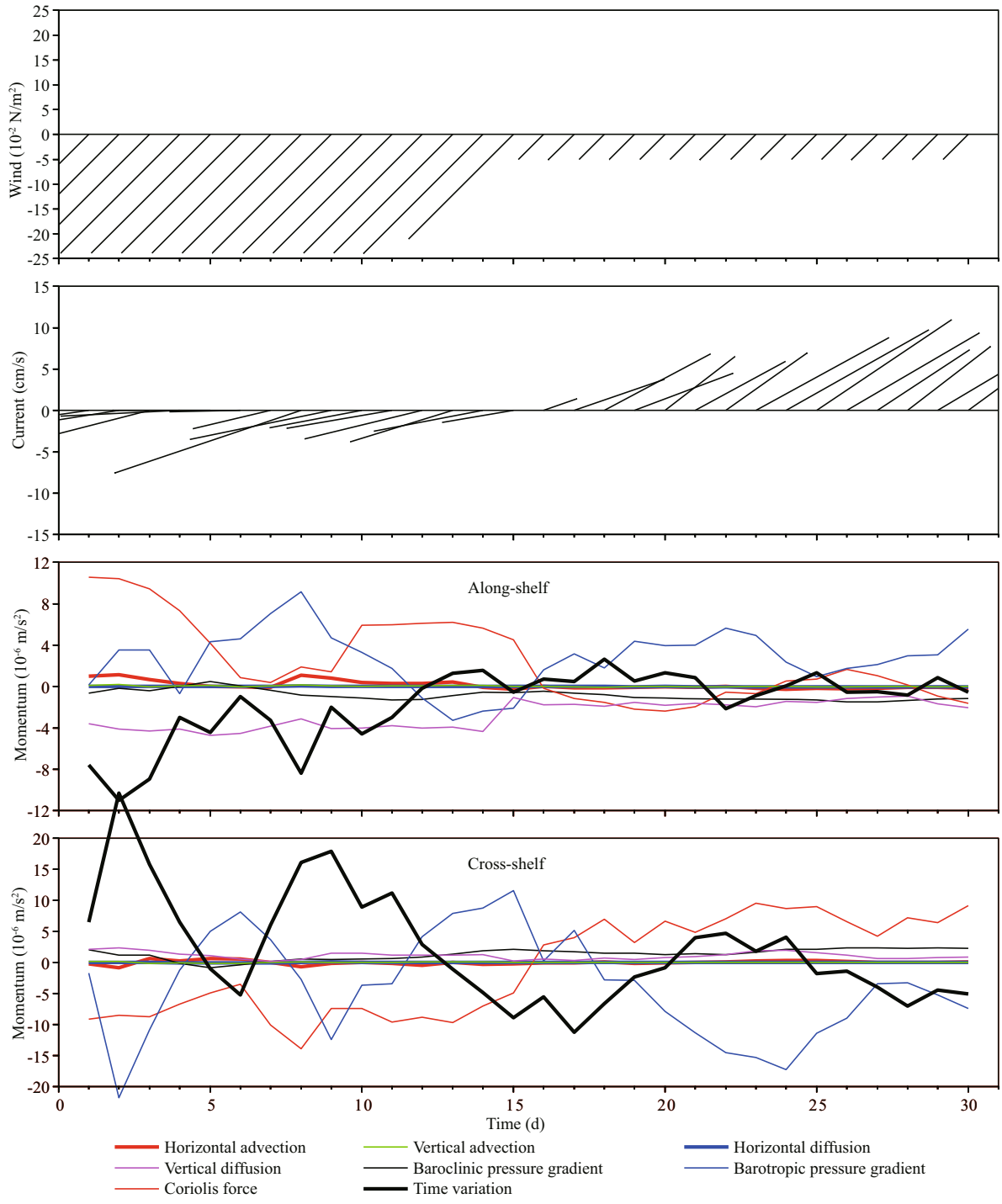

Fig.7 Time series of model-computed daily wind stress, current vectors and along- and cross-shelf momentum balance terms along the transect located west of the Zhujiang River estuary for January 2002

time-distance distributions of the model-computed current vectors at 10 m depth along the transect, superimposed on the along- and cross-shelf pressure gradient contours. Along the transect, the surface currents generally flow westward before wind relaxation. During the first days of the wind relaxation (from 16 to 18 January), the surface currents having an offshore distance of 70–230 km turn from westward to northeastward; simultaneously, the along-shelf pressure gradient in these areas also turns toward the same direction. The rotation of the currents breaks the quasi-geostrophic balance in the cross-shelf direction, while the pressure gradient decreases, but remains towards seaward, having the same direction as the

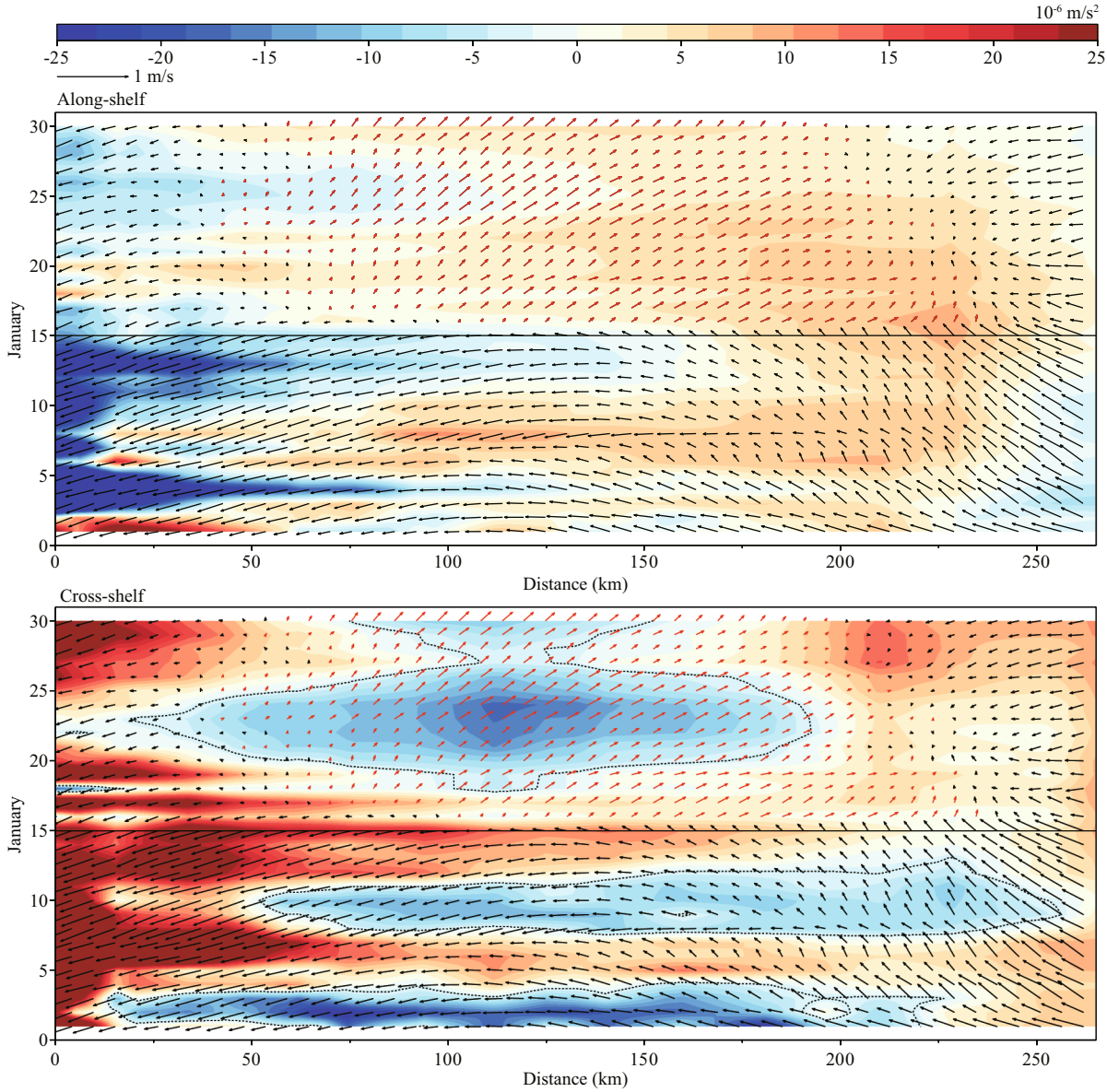

Fig.8 Variation of current vectors at 10 m depth with distance and time along the transect located west of the Zhujiang River estuary, superimposed on along- (upper panel) and cross-shelf (lower panel) pressure gradients

The contours indicate a pressure gradient of zero. Northeastward along-shelf and seaward cross-shelf directions are defined as positive in this study.

Coriolis force induced by the northeastward currents. The superposition of the cross-shelf pressure gradient and Coriolis force compels the currents to rotate clockwise, and the continuously positive along-shelf pressure gradient accelerates the northeastward current. In the following period (from 20 to 30 January), the maintenance of the northeastward SCSWC generally depends on the balance between the cross-shelf pressure gradient and Coriolis force, while the intensity of the current is related to the magnitude of the cross-shelf pressure gradient. This can be seen for vectors with an offshore distance of 75–175 km from 22 to 27 January.

The model results and the momentum budget suggest that the northeastward pressure gradient along-shelf provides the initial driving force for the northeastward SCSWC. This gradient plays a significant role in the startup process of the SCSWC, driving the current to change direction. With accompanying sea level change over the shelf, the SCSWC gradually adjusts to a quasi-geostrophic balance, reaching steady state. Hence, the balance between the pressure gradient and Coriolis force in the cross-shelf direction becomes the primary dynamic mechanism of maintaining the SCSWC during this period.

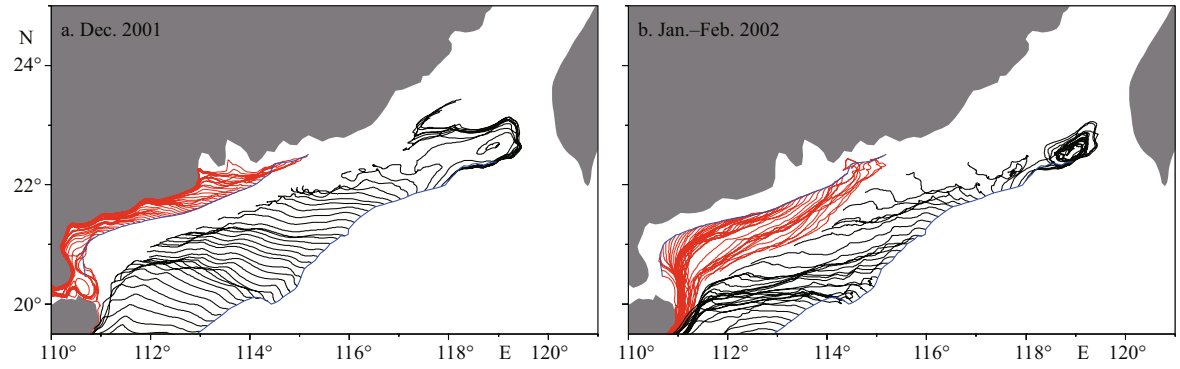

Fig.9 Trajectories of particles released at 10 m depth along the 30- and 200-m isobaths for December 2001 (a) and from January to February 2002 (b)

Blue lines denote the initial positions of particles before release. Red and black lines indicate trajectories of particles released along 30- and 200-m isobaths, respectively.

3.5 Lagrangian particle tracking experiments

Besides water transport induced by the northeasterly monsoon, the cross-shelf transport related to the southwestward slope current also makes a great contribution to sea level over the shelf (Hong and Wang, 2006; Wang et al., 2010). Lagrangian particle tracking experiments were carried out to determine the contribution of the southwestward slope current and coastal current to the SCSWC, using our numerical model.

To mark the approximate locations of the coastal and slope currents, the isobaths of 30 and 200 m were selected as the initial positions for particle release (blue lines, Fig.9). The particles were fixed at 10 m depth, and were released on 1 December 2001 (having a strong northeasterly wind condition) and 20 January 2002 (having a weak northeasterly wind condition), respectively. The corresponding trajectories of these particles are shown in Fig.9. When the winter monsoon was strong, particles over the shelf break moved northwestward (Fig.9a), indicating that part of the slope current turned shoreward. Similarly, particles within the southwestward coastal current also deviated to the northwest during this period. Typically, a strong northeasterly wind induces significant shoreward Ekman transport, which facilitates high sea level in the northeastern SCS, but not in the mid-shelf region. Particles released around the 30-m isobath moved southwestward, while those released around the 200-m isobath moved northwestward during wind relaxation (Fig.9b). The shoreward transport of the southwestward slope current decreased in our simulation. As a result, water converged over the shelf to generate a high sea level band in the mid-shelf region, favoring formation of the SCSWC by providing a source of mass.

4 CONCLUSION

Recent current measurements from moored ADCPs are useful to characterize subtidal currents over the NSCS continental shelf and shelf break. They show that winter circulation over the shelf is mainly southwestward flow driven by the northeasterly monsoon, with the episodic effects of mesoscale eddies propagating westward along isobaths. However, the persistent northeastward SCSWC is not observed in these measurements, despite the fact that currents over the shelf region do respond to winter monsoon relaxation, as described in previous observations.

Our numerical model, based on a Finite-Volume Community Ocean Model, reproduces the Kuroshio intrusion through the Luzon Strait and surface circulation in the NSCS at a high-resolution time scale, and captures the characteristics and variations of the subtidal current. We conclude that the SCSWC is not a permanent winter feature, according to our model-data comparison of the circulation patterns and subtidal currents over the winter periods of a number of years. Our model indicates that for a case study of January 2002, the currents over the NSCS continental shelf were generally southwestward, while the winter monsoon was strong, but gradually became northeastward, once the wind attenuated. Typically, the SCSWC occurs between 50- and 100-m isobaths, with prominent temporal and spatial variations linked to the northeasterly monsoon.

A numerical experiment was carried out in this study to examine the response of the currents over the NSCS continental shelf to wind relaxation. Our results show that sea level becomes elevated in the northwestern SCS, because of Ekman transport, induced by the persistent northeasterly monsoon.

Following wind relaxation, built-up water flows southeastward to form a high sea level band around the mid-shelf, generating along- and cross-shelf pressure gradients. The SCSWC subsequently develops, having a maximum velocity of 30 cm/s at the surface and a strong vertical barotropic character. The momentum budget along a transect, located west of the Zhujiang River estuary, shows that the barotropic pressure gradient term is dominant in both along- and cross-shelf directions. The along-shelf pressure gradient is towards the northeast, and provides the initial driving force for the SCSWC during the first few days after relaxation of the monsoon wind. With ongoing adjustment of sea level over the shelf, the shoreward cross-shelf pressure gradient gradually balances the Coriolis force induced by the northeastward SCSWC. The current ultimately reaches a steady quasi-geostrophic balance in the cross-shelf direction.

Our Lagrangian particle tracking experiments indicate that following wind relaxation, the transport of the southwestward coastal current and slope current towards the mid-shelf facilitates the northeastward SCSWC, and provides a mass source for the SCSWC.

5 ACKNOWLEDGEMENT

We thank the Ocean University of China's Physical Oceanography Laboratory Ocean Data and Simulation Center for providing the hardware support. We also thank Asia-Pacific Data-Research Center (APDRC) of the International Pacific research Center, Center for Earth Information Science and Technology (CEIST), Geophysical Fluid Simulation Research Group (GFSG), NASA's Making Earth Science data records for Use in Research Environments (MEaSUREs) Program, NOAA's National Center for Environmental Information (NCEI), and the China Argo Real-time Data Center for providing valuable data for this study.

References

Centurioni L R, Niiler P N, Lee D K. 2009. Near-surface circulation in the South China Sea during the winter monsoon. *Geophys*. *Res*. *Lett*., **36**(6): L06605, https://doi.org/10.1029/2008GL037076.

Chao S Y, Shaw P T, Wang J. 1995. Wind relaxation as possible cause of the South China Sea Warm Current. *J*. *Oceanogr*., **51**(1): 111-132.

Chen K, He R. 2015. Mean circulation in the coastal ocean off northeastern North America from a regional-scale ocean model. *Ocean*. *Sci*., **11**(4): 503-517, https://dx.doi.org/10.5194/os-11-503-2015.

Chiang T L, Wu C R, Chao S Y. 2008. Physical and geographical origins of the South China Sea Warm Current. *J*. *Geophys*. *Res*., **113**(C8): C08028, https://doi.org/10.1029/2008JC004794.

Chu P C, Fan C W, Lozano C J, Kerling J L. 1998. An airborne expendable bathythermograph survey of the South China Sea, May 1995. *J*. *Geophys*. *Res*., **103**(C10): 21 637-21 652.

Fang G H, Zhao B R. 1988. A note on the main forcing of the northeastward flowing current off the Southeast China Coast. *Progress in Oceanography*, **21**(3): 363-372.

Guan B X, Chen S J. 1964. The Current Systems in the Near-sea Area of China Seas. Initial Report 5. Institute of Oceanology, Chinese Academy of Sciences, Qingdao, China. p.1-85. (in Chinese)

Guan B X, Fang G H. 2006. Winter counter-wind currents off the southeastern China coast: a review. *J*. *Oceanogr*., **62**(1): 1-24.

Guan B X. 1978. The warm current in the South China Sea-a current flowing against the wind in winter in the open sea off Guangdong Province. *Oceanol*. *Limnol*. *Sin*., **9**(2): 117-127. (in Chinese with English abstract)

Guan B X. 1985. Some features of the temporal and spatial distributions of the "counter-wind" current in northern South China Sea in winter. *Oceanol*. *Limnol*. *Sin*., **16**(6): 429-438. (in Chinese with English abstract)

Guan B X. 1986. Evidence for a counter-wind current in winter off the southeast coast of China. *Chin*. *J*. *Oceanol*. *Limnol*., **4**(4): 319-332.

Guan B X. 2002. Winter Counter-Wind Current off the Southeastern China Coast. China Ocean University Press, Qingdao, China. 267p. (in Chinese)

Guo Z X, Yang T H, Qiu D Z. 1985. The South China Sea warm current and the SW-ward current on its right side in winter. *Tropical Oceanology*, **4**(1): 1-9. (in Chinese with English abstract)

He Q, Wei Z X, Wang Y G. 2012. Study on the sea currents in the northern shelf and slope of the South China Sea based on the observation. *Acta*. *Oceanol*. *Sin*., **34**(1): 17-28. (in Chinese with English abstract)

Hong B, Wang D X. 2006. Diagnostic analysis on the northern South China Sea winter counter-wind current. *Chinese Science Bulletin*, **51**(2): 9-16.

Hsueh Y, Zhong L J. 2004. A pressure-driven South China Sea warm current. *J*. *Geophys*. *Res*., **109**(C9): C09014, https://doi.org/10.1029/2004JC002374.

Li L, Nowlin Jr W D, Su J L. 1998. Anticyclonic rings from the Kuroshio in the South China Sea. *Deep Sea Res*. *I*, **45**(9): 1 469-1 482.

Li R X, Chen C S, Xia H Y, Beardsley R C, Shi M C, Lai Z G, Lin H C, Feng Y Q, Liu C J, Xu Q C, Ding Y, Zhang Y. 2014. Observed wintertime tidal and subtidal currents over the continental shelf in the northern South China Sea. *J*. *Geophys*. *Res*., **119**(8): 5 289-5 310, https://doi.org/10.1002/2014JC009931.

Mellor G L, Yamada T. 1982. Development of a turbulence closure model for geophysical fluid problems. *Rev*. *Geophys*., **20**(4): 851-875.

Smagorinsky J. 1963. General circulation experiments with the primitive equations: I. The basic experiment. *Mon. Wea. Rev.*, **91**(3): 99-164.

Su J L, Liu X B. 1992. Numerical simulation of circulation in the South China Sea. *In*: Zeng Q C ed. Proceedings of Symposium on Ocean Circulation. China Ocean Press, Beijing, China. p.206-215. (in Chinese)

Su J L, Wang W. 1987. On the sources of the Taiwan warm current from the South China Sea. *Chin. J. Oceanol. Limnol.*, **5**(4): 299-308.

Su J Z, Lu J, Hou Y J, fang G H, Wei Z X, Yin B S. 2002. Analysis of satellite-tracked drifting buoys in the South China Sea. *Oceanol. Limnol. Sin.*, **33**(2): 121-127. (in Chinese with English abstract)

U.S. Naval Oceanographic Office and the U.S. 1983. Naval Ocean Research and Development Activity. DBDB5 (Digital Bathymetric Data Base-5 Minute Grid). U. S. Naval Oceanographic Office, Bay St. Louis. 329p.

Wang D X, Hong B, Gan J P, Xu H Z. 2010. Numerical investigation on propulsion of the counter-wind current in the northern South China Sea in winter. *Deep Sea Res. I*, **57**(10): 1 206-1 221.

Wang D X, Xu H Z, Lin J, Hu J Y. 2008. Anticyclonic eddies in the northeastern South China Sea during winter 2003/2004. *J. Oceanogr.*, **64**(6): 925-935, https://doi.org/10.1007/s10872-008-0076-3.

Wang K, Fang G H, Shi X H. 2001. Numerical study on the formation of the South China Sea Warm Current II. Baroclinic Case. *Chin. J. Oceanol. Limnol.*, **19**(4): 306-311.

Wang K, Fang Y. 2001. Numerical study on the formation of the South China Sea warm current I. Barotropic case. *Chin. J. Oceanol. Limnol.*, **19**(1): 1-9.

Wang Q, Wang Y X, Bo H, Zhou W D, Wang D X. 2011. Different roles of Ekman pumping in the west and east segments of the South China Sea Warm Current. *Acta. Oceanol. Sin.*, **30**(3): 1-13.

Wyrtki K. 1961. Physical oceanography of the Southeast Asian water. *In*: Wyrtki K ed. NAGA Report: Scientific Result of Marine Investigation of the South China Sea and Gulf of Thailand 1959-1961. Scripps Institution of Oceanography, California, United States. p.155-160.

Xie J P, Zhu J. 2008. Estimation of the surface and mid-depth currents from Argo floats in the pacific and error analysis. *J. Mar. Syst.*, **73**(1-2): 61-75.

Xie J P, Zhu J. 2009. A dataset of global ocean surface currents for 1999-2007 derived from Argo float trajectories: a comparison with Surface Drifter and TAO measurements. *Atmos. Ocean. Sci. Lett.*, **2**(2): 97-102.

Xiong X J. 2013. The circulation structure and mechanism studies on the China Seas. Ocean University of China, Qingdao, China. 208p. (in Chinese)

Xue H J, Chai F, Pettigrew N, Xu D Y, Shi M C, Xu J P. 2004. Kuroshio intrusion and the circulation in the South China Sea. *J. Geophys. Res.*, **109**(C2): C02017, https://doi.org/10.1029/2002JC001724.

Yang J Y, Wu D X, Lin X P. 2008. On the dynamics of the South China Sea warm current. *J. Geophys. Res.*, **113**(C8): C08003, https://doi.org/10.1029/2007JC004427.

Yang K C. 2006. The non-persistent South China Sea warm current. National Taiwan University, Taipei, China. 49p.

Yuan D L, Han W Q, Hu D X. 2007. Anti-cyclonic eddies northwest of Luzon in summer-fall observed by satellite altimeters. *Geophys. Res. Lett.*, **34**(13): L13610, https://doi.org/10.1029/2007GL029401.

Zeng X Z, Peng S Q, Li Z J, Qi Y Q, Chen R Y. 2014. A reanalysis dataset of the South China Sea. *Sci. Data.*, **1**: 140052. https://doi.org/10.1038/sdata.2014.52.

Zhong H L. 1990. Structures of the density circulation. *In*: Ma Y L ed. Report of Decadal Hydrographic Series Survey of the Shelf and Adjacent Waters of the Northern South China Sea. China Ocean Press, Beijing, China. p.215-241. (in Chinese)